

Enhanced Corrosion Resistance of Carbon Steel in Hydrochloric Acid Solution by Polyoxometalate-Estertin Derivatives

Xing-Fang Wang,[#] Xin-Yu Liu,[#] Fang Su, Jian-Sheng Li, Zai-Ming Zhu,^{*} Xiao-Jing Sang,^{*} and Lan-Cui Zhang^{*}



Cite This: *ACS Omega* 2022, 7, 4429–4443



Read Online

ACCESS |



Metrics & More

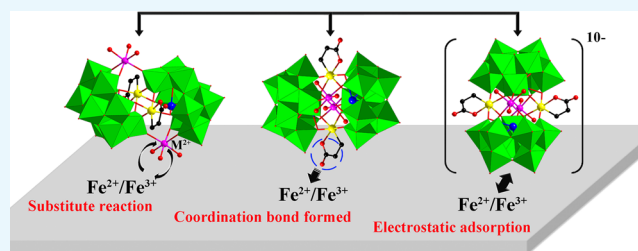


Article Recommendations



Supporting Information

ABSTRACT: The development of acid-resistant and efficient corrosion inhibitors is of great significance for metal protection in many industrial processes. In this work, eight cases of sandwich-type polyoxometalate (POM)-based inorganic–organic hybrids, namely, carboxyethyltin and transition metal (TM) cofunctionalized tungstoantimonates and tungstobismuthates, formulated as $\text{Na}_x\text{K}_{10-x}[(\text{SnR})_2(\text{TM}(\text{H}_2\text{O})_3)_2(\text{B}-\beta\text{-SbW}_9\text{O}_{33})_2]\cdot m\text{H}_2\text{O}$ and $\text{Na}_y\text{K}_{10-y}[(\text{SnR})_2(\text{TM}(\text{H}_2\text{O})_3)_2(\text{B}-\beta\text{-BiW}_9\text{O}_{33})_2]\cdot n\text{H}_2\text{O}$ (abbreviated as **SbW₉-TM-SnR** and **BiW₉-TM-SnR**; TM = Mn, Co, Ni, and Zn; $m = 18, 24, 24,$ and 22 ; $n = 30, 25, 20,$ and 21 ; SnR = $\text{Sn}(\text{CH}_2\text{CH}_2\text{COO})$) are first used as green corrosion inhibitors for 20[#] carbon steel in 0.5–2.0 M HCl solutions. Weight loss and electrochemical experiments prove that the corrosion inhibition efficiency is all above 81% for these POM-based corrosion inhibitors at 150 mg L⁻¹, and **SbW₉-Mn-SnR** shows the highest efficiency of 96.9% at 150 mg L⁻¹ after immersion in a 0.5 M HCl solution for 10 h. Scanning electron microscopy–energy-dispersive X-ray spectroscopy and X-ray photoelectron spectroscopy analyses show that these POM-based inhibitors form films on the carbon steel and the adsorption mechanism obeys the Langmuir adsorption model. The thermodynamic activation parameters were calculated, proving the occurrence of both chemical and physical adsorptions. The film-forming mechanism was also analyzed. This work provides guidance for synthesizing new lacunary POM-based materials to protect metals from corrosion in HCl pickling.



INTRODUCTION

Metal anticorrosion is of great significance in fields of industrial production and environmental protection because oxygen or acid corrosion of metals is a spontaneous chemical reaction, which will increase energy consumption of equipment and cause leakage of oil or gas from pipelines in industry. Several strategies have been used to protect metals against corrosion, such as photoinduced cathodic protection and adding corrosion inhibitors.¹ Adsorptive corrosion inhibitors have attracted intensive attention because of their excellent performance and operational ease. In addition, it is well-known that the fastest and most effective way to remove rust and scale from equipment is acid pickling, and hydrochloric acid is one of the most commonly used pickling solution. However, HCl solution is highly corrosive to metallic equipment, so a suitable corrosion inhibitor needs to be added in a chemical acidic cleaning process of equipment.^{2,3} In the early stage, some simple oxysalts were used for metal corrosion inhibition, but they are mostly used in neutral media rather than acidic solution.^{4,5} For organic corrosion inhibitors, they have more obvious advantages in acidic media.⁶ For instance, ionic liquids (ILs) have shown their outstanding performance in corrosion inhibition of steels in the acidic environment owing to many attractive characteristics such as high stability, high solubility, and low environmental hazards,

although they suffer from the high production cost sometimes.^{7,8} Moreover, plant extract corrosion inhibitors have been widely studied as green corrosion inhibitors owing to their high inhibition efficiency, chemical stability, and environmental friendliness. However, their application is limited by the difficulty of separation.^{9–11} In recent years, intelligent corrosion inhibitors with pH responsivity, self-assembly, and self-healing properties have attracted more and more attention of scientists.^{12–16} Despite the above achievements, the development of new sustainable, environmentally friendly, and highly efficient corrosion inhibitors in acidic media is still an important topic in metal protection.

POMs, as a kind of well-defined and nano-sized anionic metal-oxygen cluster possessing low toxicity, high electron affinity, and structural stability, have been widely applied in energy-related fields.^{17,18} Such excellent properties also make them attractive as oxidizing and film-forming corrosion inhibitors.¹⁹ In 1994,

Received: November 8, 2021

Accepted: January 10, 2022

Published: January 25, 2022



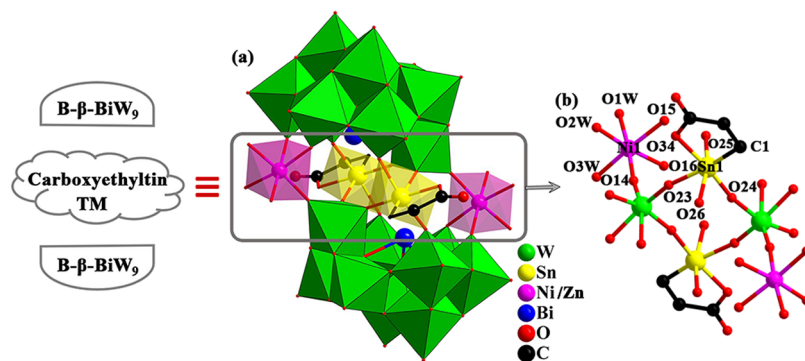


Figure 1. Polyhedral and ball-and-stick representation of the BiW₉-Ni/Zn-SnR polyoxoanion (a) and ball-and-stick diagram corresponding to the central belt (b) (H atoms, K⁺, Na⁺, and free H₂O molecules have been omitted for clarity).

Lomakina *et al.* used several heteropolytungstates as corrosion inhibitors of aluminum and alloys in high-temperature water.²⁰ Liang *et al.* found that Na₃PW₁₂O₄₀ and H₄PW₁₁VO₄₀ could effectively retard the corrosion of carbon steel in 55% LiBr solution.^{21,22} Hamdani *et al.* reported that hexa-ammonium heptamolybdate tetrahydrate could act as an anode corrosion inhibitor for 304 stainless steel in 0.5 M HCl solution, and the inhibition efficiency could reach above 90%.²³ In addition, research on POM-based composites as metal corrosion inhibitors has been increasingly conducted. Cases Iborra *et al.* reported that polypyrrole/PW₁₂O₄₀³⁻ coatings protect carbon steel electrodes against corrosion in chloride aqueous solutions.²⁴ According to the work reported by Rao *et al.*, the ferrocene POM hybrid molecular materials show significant corrosion inhibition performance when coated on stainless steel plates (SS, 316 grade) in 0.5 M H₂SO₄ and Ringer's solutions.¹⁹ The hydrophobic POM-ILs composed of organic bulk cations and inorganic anions through weak interaction are also excellent corrosion-protection coating of metal surfaces in acetic acid or H₂SO₄ solutions.^{25,26} They can also protect typical building stones from corrosion (weathering) and biofilm formation (biodeterioration).²⁷ Although many POMs or POM-based composite materials as metal corrosion inhibitors have been studied, relatively few studies have been conducted on POM inhibitors for carbon steel in HCl pickling, especially for lacunary POMs.

As everyone knows, the introduction of organic or organometallic groups can enhance POM's functions and stabilize the structures. Organotin, including alkyltin and estertin/carboxyltin, possesses some unique properties and is the most widely used organometallic compounds. In 1989, Mourad *et al.* found that dimethyltin dichloride could form an adsorption film on an aluminum surface in a HCl medium, exhibiting effective corrosion inhibition.²⁸ In view of low toxicity, high stability, functionality of estertin/carboxyltin, and the versatility of POMs, the first single crystal of carboxyethyltin-modified POM was obtained in 2010.²⁹ After that, sandwich-type tungstoarsenate and tungstogermanate containing carboxyethyltin groups were synthesized and studied as corrosion inhibitors on carbon steel in circulating cooling water systems.^{30,31} In order to further investigate the corrosion inhibition behavior of this series of sandwich-type POMs to carbon steel in acidic solutions, in this work, two new sandwich-type tungstobismuthates Na₅K₅[(Sn(CH₂CH₂COO))₂(Ni(H₂O)₃)₂(B-β-BiW₉O₃₃)₂]·20H₂O (BiW₉-Ni-SnR) and Na₅K₅[(Sn(CH₂CH₂COO))₂(Zn(H₂O)₃)₂(B-β-BiW₉O₃₃)₂]·21H₂O (BiW₉-Zn-SnR) were newly synthesized in aqueous

media. The corrosion inhibition activity of the two new compounds and other six sandwich-type POMs (SbW₉-TM-SnR, TM = Mn, Co, Ni, and Zn; BiW₉-TM-SnR, TM = Mn and Co),^{32,33} was all evaluated by weight loss, potentiodynamic polarization testing, electrochemical impedance spectroscopy (EIS), scanning electron microscopy (SEM), and energy-dispersive X-ray spectrometry (EDX). Moreover, the corrosion inhibition mechanism was further studied.

RESULTS AND DISCUSSION

Structural Analysis. Single-crystal X-ray structural analysis indicates that the polyoxoanions of BiW₉-Ni-SnR and BiW₉-Zn-SnR are isomorphic, and the configurations of the two POM anion skeletons are the same as those of BiW₉-Mn/Co-SnR. That is, they also consist of two trivalent Keggin [B-β-BiW₉O₃₃]⁹⁻ (B-β-BiW₉) subunits, sandwiching two Ni²⁺/Zn²⁺ ions and two SnR groups, displaying the well-known Keggin sandwich-type structural features (Figure 1a). The detailed crystallographic data, data collection, and structural refinement parameters of BiW₉-Ni/Zn-SnR are summarized in the supporting materials (Table S1). In the synthesis of the two POMs, it is also found that some similar phenomena occur, i.e., the configuration of the starting material B-α-BiW₉ changes to B-β-BiW₉, and the raw material estertin [SnCH₂CH₂COOCH₃]³⁺ hydrolyzes to carboxyethyltin [SnCH₂CH₂COO]²⁺ (Scheme S1), but its original five-membered ring is not opened. As shown in Figure 1b, in the central belt of the sandwich-type POM anion, each Ni/Zn center is six-coordinated with three terminal O atoms (O14, O15, and O16) from three WO₆ octahedra and three other O atoms (O1W, O2W, and O3W) of three H₂O molecules. Each Sn atom also displays a six-coordinated configuration with four terminal O atoms (O23, O24, O25, and O26) from four WO₆ octahedra and one C atom (C1) and one O atom (O34) from a [SnCH₂CH₂COO]²⁺ group. In the two POMs, the adjacent polyoxoanions are connected by electrostatic interaction with counterions Na⁺ and K⁺ and hydrogen bondings with free H₂O molecules to form 3-D network structures (Figure S1). The selected bond lengths and angles of the two POMs are listed in Tables S2 and S3.

The structure and thermal stability of BiW₉-Ni-SnR and BiW₉-Zn-SnR were further characterized by IR, powder X-ray diffraction patterns (PXRD), and thermogravimetric (TG) analysis (Figures S2–S4). The detailed analysis can be found in the supplementary materials. These analytical results are consistent with the results of single-crystal structure analysis,

and TG results show that the main POM skeletons of the two new compounds still exist at about 750 °C.

Gravimetric Evaluation of Metal Corrosion. The weight loss method was used to evaluate the corrosion rate and inhibition efficiency (IE_w) of 20[#] carbon steel in 0.5–2.0 M HCl solutions at room temperature without and with different POM-based corrosion inhibitors. The corrosion rate was calculated according to eq 1:³⁴

$$C_R = \frac{\Delta m}{s \times \Delta t} \quad (1)$$

where C_R ($\text{mg cm}^{-2} \text{h}^{-1}$) is the corrosion rate; Δm (mg) and Δt (h) are the average weight loss of 20[#] carbon steel immersed in HCl solutions by multiple tests and the immersion time, respectively; s (12.6 cm^2) is the area of the 20[#] carbon steel sample; IE_w was obtained using eq 2:³⁴

$$IE_w(\%) = \left[1 - \frac{W_{\text{cor}}}{W_{\text{cor}}^0} \right] \times 100 \quad (2)$$

W_{cor} and W_{cor}^0 are the weight losses with and without the POM-based inhibitor, respectively.

Taking **SbW₉-Mn-SnR** for example, the optimal concentration of the POM-based corrosion inhibitor for 20[#] carbon steel in 0.5 M HCl solution for 6 h at room temperature was investigated (Table 1). As shown in Table 1, with increasing the

Table 1. Corrosion Parameters Obtained from the Weight Loss Measurements for 20[#] Carbon Steel Immersed in 0.5 M HCl Solution with Different Concentrations of SbW₉-Mn-SnR for 6 h at Room Temperature (298 K)

concentration (mg L^{-1})	Δm (g) ^a	C_R ($\text{mg cm}^{-2} \text{h}^{-1}$)	IE_w (%)
	0.0474	0.627	
25	0.0094	0.124	80.2
75	0.0062	0.082	86.9
150	0.0048	0.063	89.9
300	0.0046	0.044	90.3

^aNote: Δm is the average weight loss by multiple tests.

inhibitor concentration (from 25 to 300 mg L^{-1}), the value of IE_w gradually increases (from 80.2 to 90.3%). However, at higher concentrations, i.e., the concentration of **SbW₉-Mn-SnR** is from 150 to 300 mg L^{-1} , the value of IE_w only increases by 0.4% (from 89.9 to 90.3%).

In order to further investigate the effects of concentration and immersion time on the inhibitory behaviors of inhibitors, the inhibition performances of various inhibitors including **SbW₉-TM-SnR**, **BiW₉-TM-SnR** (TM = Mn, Co, Ni, and Zn), and their parent compounds (**Na-SbW₉** and **Na-BiW₉**) at higher concentrations (300 and 500 mg L^{-1}) toward the corrosion of 20[#] carbon steel immersed in 0.5 M HCl solution for 6 and 10 h at room temperature were evaluated (Table 2 and Table S4). As seen from Table 2, for **SbW₉-TM-SnR** and **BiW₉-TM-SnR**, when the inhibitor concentration increases from 300 to 500 mg L^{-1} after immersion in 0.5 M HCl solution for 6 h, there are no significant increases on the values of IE_w for all inhibitors, which may be attributed to the saturation adsorption of inhibitors on the surface of 20[#] carbon steel. When the immersion time extends from 6 to 10 h, the IE_w values of **SbW₉-TM-SnR** (TM = Mn, Co, Ni, and Zn) at 300 mg L^{-1} increase from 92.9, 91.5, 92.3, and 90.4% to 93.2, 93.1, 93.8, and 94.0% and the IE_w values of **BiW₉-TM-SnR** (TM = Mn, Co, Ni, and Zn) increase from

Table 2. Corrosion Parameters Obtained from Weight Loss Measurement for 20[#] Carbon Steel Immersed in 0.5 M HCl Solution Containing Various Inhibitors at Different Concentrations for 6 and 10 h at Room Temperature (301 K)

inhibitor	concentration (mg L^{-1})	time (h)	Δm (g) ^a	C_R ($\text{mg cm}^{-2} \text{h}^{-1}$)	IE_w (%)
blank		6	0.0520	0.688	
		10	0.0912	0.724	
SbW₉-Mn-SnR	300	6	0.0037	0.049	92.9
		10	0.0062	0.049	93.2
SbW₉-Co-SnR	300	6	0.0042	0.056	91.9
		10	0.0044	0.058	91.5
SbW₉-Ni-SnR	300	6	0.0046	0.061	91.2
		10	0.0040	0.053	92.3
SbW₉-Zn-SnR	300	6	0.0057	0.045	93.8
		10	0.0038	0.050	92.7
BiW₉-Mn-SnR	300	6	0.0050	0.066	90.4
		10	0.0055	0.044	94.0
BiW₉-Co-SnR	300	6	0.0047	0.062	90.7
		10	0.0082	0.108	84.3
BiW₉-Ni-SnR	300	6	0.0102	0.081	87.8
		10	0.0080	0.106	85.9
BiW₉-Zn-SnR	300	6	0.0093	0.123	82.2
		10	0.0106	0.084	87.4
Na-SbW₉	300	6	0.0077	0.102	86.4
		10	0.0073	0.097	86.0
Na-BiW₉	300	6	0.0111	0.088	86.7
		10	0.0082	0.108	85.6
Na-SbW₉	500	6	0.0078	0.103	85.0
		10	0.0104	0.083	87.5
Na-BiW₉	500	6	0.0068	0.090	88.0

^aNote: Δm is the average weight loss by multiple tests.

84.3, 82.2, 86.0, and 85.0% to 87.8, 87.4, 86.7, and 87.5%, respectively. Meanwhile, the C_R values of carbon steel all decrease for the eight inhibitors, indicating that the adsorption films of inhibitors are stable. For **Na-SbW₉** and **Na-BiW₉**, the IE_w values are far less than those of **SbW₉-TM-SnR** and **BiW₉-TM-SnR** (Table S4). Based on the above experimental results and energy consumption reduction consideration, the latter experiments were performed at 298 K, an immersion time of 6 h, and an inhibitor concentration of 150 mg L^{-1} . Under the optimal conditions, the corrosion inhibition effect of different POM-based inhibitors on 20[#] carbon steel immersed in 0.5–2.0 M HCl solutions was evaluated and is summarized in Table 3.

As shown in Table 3, in 0.5–2.0 M HCl solutions, the IE_w values of these sandwich-type POM-based inhibitors containing the same SnR and different TMs are similar and all higher than 81%, which is obviously higher than those of parents **Na-SbW₉** (11.4–26.5%) and **Na-BiW₉** (9.1–34.3%). The above results show that these POM-based inhibitors have good corrosion inhibition performance for carbon steel in acidic solutions, and the type of TM component has little effect on the corrosion inhibition property. It is noted that the IE_w values of **SbW₉-TM-SnR** and **BiW₉-TM-SnR** are slightly reduced in 2.0 M HCl compared to those in 1.0 M HCl, which is presumed to be because (i) a high concentration of Cl^- penetrates the anticorrosive film and causes repitting corrosion and (ii) the corrosion film dissolves or decomposes.³⁵ In addition, the corrosion inhibition performance of **SbW₉-TM-SnR** is slightly better than that of **BiW₉-TM-SnR**. It can also be seen from

Table 3. Corrosion Parameters Obtained from the Weight Loss Measurement for 20[#] Carbon Steel Immersed in 0.5, 1.0, and 2.0 M HCl Solutions Containing 150 mg L⁻¹ Different Inhibitors for 6 h at 298 K

inhibitor	HCl solution concentration (M)	Δm (g) ^a	C_R (mg cm ⁻² h ⁻¹)	IE _w (%)
blank	0.5	0.0473	0.626	
	1.0	0.0615	0.813	
	2.0	0.0829	1.097	
SbW ₉ -Mn-SnR	0.5	0.0048	0.063	89.9
	1.0	0.0039	0.052	93.6
	2.0	0.0109	0.144	86.8
SbW ₉ -Co-SnR	0.5	0.0048	0.063	89.8
	1.0	0.0045	0.060	92.7
	2.0	0.0121	0.160	85.4
SbW ₉ -Ni-SnR	0.5	0.0046	0.061	90.3
	1.0	0.0056	0.074	90.9
	2.0	0.0115	0.152	86.1
SbW ₉ -Zn-SnR	0.5	0.0049	0.065	89.6
	1.0	0.0053	0.070	91.4
	2.0	0.0106	0.140	87.2
BiW ₉ -Mn-SnR	0.5	0.0084	0.111	82.2
	1.0	0.0061	0.081	90.1
	2.0	0.0112	0.148	86.5
BiW ₉ -Co-SnR	0.5	0.0086	0.114	81.8
	1.0	0.0061	0.081	90.1
	2.0	0.0118	0.156	85.8
BiW ₉ -Ni-SnR	0.5	0.0074	0.098	84.4
	1.0	0.0054	0.071	91.2
	2.0	0.0120	0.159	85.5
BiW ₉ -Zn-SnR	0.5	0.0073	0.097	84.6
	1.0	0.0052	0.069	91.5
	2.0	0.0111	0.147	86.6
Na-SbW ₉	0.5	0.0419	0.554	11.4
	1.0	0.0565	0.747	8.1
	2.0	0.0609	0.805	26.5
Na-BiW ₉	0.5	0.0430	0.569	9.1
	1.0	0.0509	0.067	17.2
	2.0	0.0545	0.720	34.3
Cl ₃ Sn(CH ₂) ₂ COOCH ₃	0.5	0.0060	0.079	87.3
	1.0	0.0055	0.073	91.1
	2.0	0.0127	0.168	84.7

^aNote: Δm is the average weight loss by multiple tests.

Table 3 that Cl₃Sn(CH₂)₂COOCH₃ has a good corrosion inhibition effect with IE_w values of 87.3, 91.1, and 84.7% in 0.5, 1.0, and 2.0 M HCl solutions, respectively, which shows that the organotin component plays an important role in the corrosion protection of carbon steel although its content in the POM system is low. However, when the organotin is used as a corrosion inhibitor alone, compared with the POM-estertin derivatives, the film-forming speed for Cl₃Sn(CH₂)₂COOCH₃ is faster, while its formed film is not dense and easy to rub off. Therefore, the combination of organic and inorganic components is obviously beneficial to improving the performance of POM-based inhibitors.

Potentiodynamic Polarization Measurement. Potentiodynamic polarization curves for 20[#] carbon steel in 0.5 M HCl in the presence of different concentrations of SbW₉-Mn-SnR and different inhibitors Na-SbW₉/Na-BiW₉, Cl₃Sn-(CH₂)₂COOCH₃, and SbW₉-TM-SnR/BiW₉-TM-SnR (TM = Mn, Co, Ni, and Zn) with the same concentration (150 mg L⁻¹) at 298 K are shown in Figure 2a–c, respectively. Generally, the corrosion on the surface of metals occurs through two paths, namely, the anodic reaction and the cathodic reaction, in which

the anodic reaction involves the oxidation of iron atoms and the cathodic reaction involves the reduction of H⁺. The addition of corrosion inhibitors can usually inhibit the anodic or cathodic or both reactions by forming a protective film. From the potentiodynamic polarization plots, the corrosion current density (I_{corr}) and the corrosion potential (E_{corr}) could be obtained by finding out the intersection of two tangents sketched from the cathodic and anodic curves. In addition, the anodic Tafel slope (β_a) and the cathodic Tafel slope (β_c) could be obtained. The corrosion inhibition efficiency (IE_i) was calculated from eq 3:³⁶

$$\text{IE}_i(\%) = \left[1 - \frac{I_{\text{corr}}}{I_{\text{corr}}^0} \right] \times 100 \quad (3)$$

where I_{corr} and I_{corr}^0 are the corrosion current densities with and without the POM-based inhibitors, respectively. Consequently, the corrosion parameters including I_{corr} , E_{corr} , β_a , β_c , and IE_i were calculated and are summarized in Table 4.

Figure 2a shows that both the anodic branch and the cathodic branch move to lower current densities as the concentration of

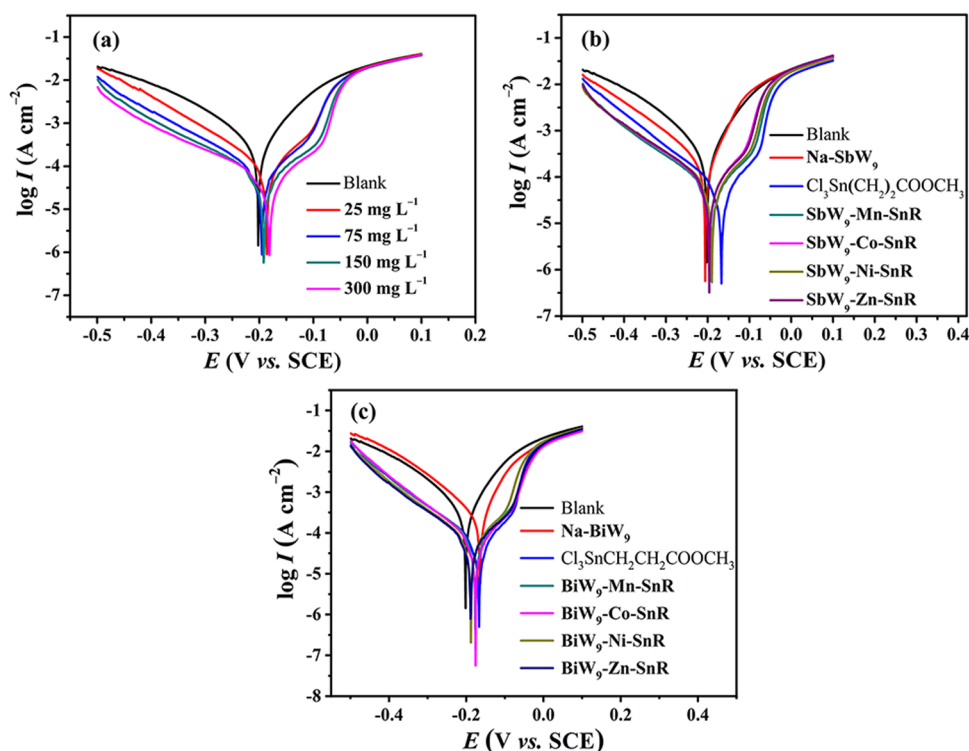


Figure 2. Potentiodynamic polarization curves for 20[#] carbon steel in 0.5 M HCl solution containing different concentrations (25, 75, 150, and 300 mg L⁻¹) of SbW₉-Mn-SnR (a) and 150 mg L⁻¹ Na-SbW₉/Na-BiW₉, Cl₃Sn(CH₂)₂COOCH₃, and SbW₉-TM-SnR/BiW₉-TM-SnR (TM = Mn, Co, Ni, and Zn) corrosion inhibitor (b,c) at 298 K (0.5 M HCl solution was used as the blank).

Table 4. Corrosion Parameters Derived from Potentiodynamic Polarization Curves of 20[#] Carbon Steel in 0.5 M HCl Solution in the Absence (Blank) and in the Presence of Different Inhibitors at 298 K

inhibitor	inhibitor concentration (mg L ⁻¹)	β_a (mV dec ⁻¹)	β_c (mV dec ⁻¹)	E_{corr} (V vs SCE)	I_{corr} ($\mu\text{A cm}^{-2}$)	IE _i (%)
blank		109.6	-139.2	-0.208	429.5	
SbW ₉ -Mn-SnR	25	51.8	-132.9	-0.186	79.4	81.5
	75	47.8	-149.1	-0.195	47.9	88.8
	150	43.0	-165.6	-0.192	35.7	91.7
	300	39.2	-188.7	-0.181	28.1	93.5
SbW ₉ -Co-SnR	150	45.6	-168.3	-0.196	45.3	89.5
SbW ₉ -Ni-SnR	150	43.7	-165.4	-0.190	39.9	90.7
SbW ₉ -Zn-SnR	150	44.0	-168.7	-0.196	47.3	89.0
BiW ₉ -Mn-SnR	150	52.1	-154.8	-0.177	47.3	88.9
BiW ₉ -Co-SnR	150	49.5	-143.2	-0.176	46.3	89.2
BiW ₉ -Ni-SnR	150	46.5	-150.8	-0.188	40.3	90.6
BiW ₉ -Zn-SnR	150	49.4	-156.5	-0.189	44.5	89.6
Na-SbW ₉	150	106.0	-146.0	-0.206	273.0	36.4
Na-BiW ₉	150	126.4	-132.7	-0.164	432.5	
Cl ₃ Sn(CH ₂) ₂ COOCH ₃	150	45.9	-146.4	-0.146	53.2	87.6

SbW₉-Mn-SnR increases, indicating a better corrosion protection of 20[#] carbon steel by increasing the concentration of SbW₉-Mn-SnR. Moreover, the value of E_{corr} moves to a more positive position when SbW₉-Mn-SnR is added. In general, the shift magnitude of E_{corr} must exceed 85 mV to classify a corrosion inhibitor as a cathodic or anodic one. Therefore, it is concluded that SbW₉-Mn-SnR acts as a mixed-type inhibitor in view of the small shift of E_{corr} (<30 mV). Furthermore, it is noted that the cathodic branch with corrosion inhibitors shows the typical Tafel behavior, while the anodic branch displays a kink, which may be related to the degree of corrosion inhibitor coverage on the surface of carbon steel.³⁷ Meanwhile, it can be observed that the anodic branch curves tend to coincide at

higher polarization potentials. This is probably because corrosion inhibitor desorption occurs when the polarization potential exceeds the desorption potential, which accelerates the metal dissolution.³⁸

As shown in Figure 2b,c, when 150 mg L⁻¹ SbW₉-TM-SnR or BiW₉-TM-SnR is added, the lower values of corrosion current density in both anodic and cathodic parts imply that SbW₉-TM-SnR or BiW₉-TM-SnR considerably inhibits the corrosion reaction of 20[#] carbon steel. In addition, the values of E_{corr} for the inhibited solution move toward the positive direction relative to the value of E_{corr} in the blank, and the shifts are less than 85 mV. These findings indicate that the POM-based inhibitors behave as

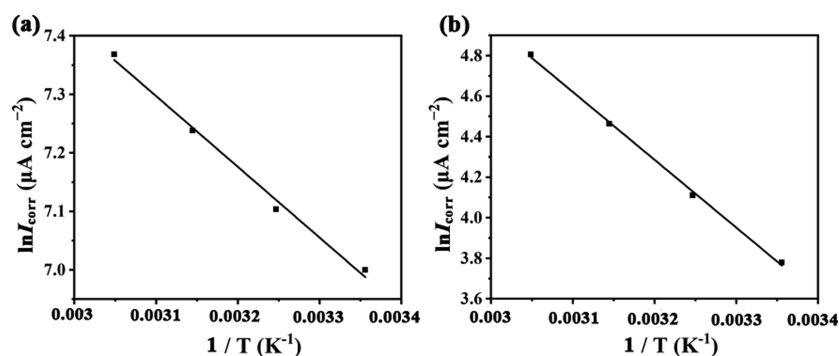


Figure 3. Arrhenius curve for 20[#] carbon steel in the presence (a) and absence (b) of SbW₉-Mn-SnR in 0.5 M HCl solution.

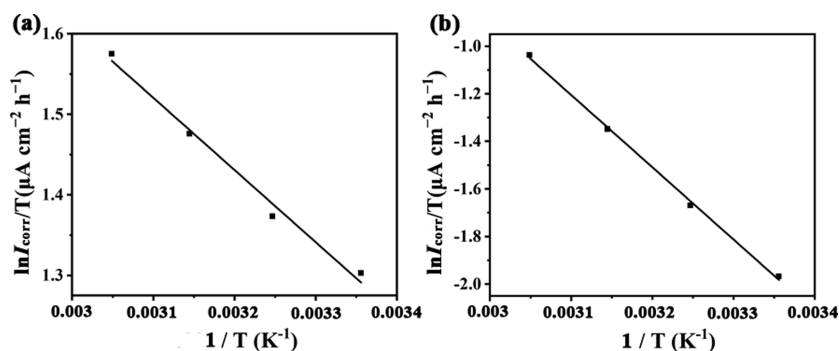


Figure 4. Transition plot for 20[#] carbon steel in the presence (a) and absence (b) of SbW₉-Mn-SnR in 0.5 M HCl solution.

mixed-type inhibitors, which inhibit both the anode metal corrosion and cathode H⁺ reduction.³⁹

As can be seen from Table 4, I_{corr} decreases with the increase in the concentration of the SbW₉-Mn-SnR inhibitor, while the IE_i increases. When the concentration of SbW₉-Mn-SnR is 300 mg L⁻¹, the IE_i can reach to 93.5%. In addition, when the dosage is only 25 mg L⁻¹, the IE_i can reach 81.5%, indicating that these inhibitors have obvious inhibition ability for 20[#] carbon steel in 0.5 M HCl at low concentration. For eight inhibitors SbW₉-TM-SnR and BiW₉-TM-SnR (TM = Mn, Co, Ni, and Zn) with a concentration of 150 mg L⁻¹, compared with starting material Na-SbW₉/Na-BiW₉, they all exhibit IE_i around 90%. The comparison results also show that SnR as a main functional group improves the corrosion inhibition performance of Na-SbW₉- or Na-BiW₉-based POMs.

In addition, the polarization curve of 20[#] carbon steel in 1.0 and 2.0 M HCl was also tested, and the results are shown in Table S5 and Figures S5 and S6. In the high concentration of HCl corrosion solutions, SbW₉-TM-SnR and BiW₉-TM-SnR can still form an adsorption film on the metal surface, and the IE_i is above 87.6%. It shows that the corrosion inhibitors have excellent acid resistance.

Thermodynamic Activation Parameters. Polarization measurements were further carried out at 298, 308, 318, and 328 K to study the influence of temperature on the corrosion process. The potentiodynamic polarization curves and corrosion parameters are shown in Figure S7 and Table S6, respectively. Accordingly, the Arrhenius plots were drawn and are presented in Figure 3, from which the apparent activation energy (E_a) could be calculated from Arrhenius equation (eq 4):⁹

$$\ln I_{\text{corr}} = \ln A - \frac{E_a}{RT} \quad (4)$$

where E_a is the activation energy at absolute temperature T (K), R epitomizes the universal gas constant of 8.314 J K⁻¹ mol⁻¹, and A is the Arrhenius factor. E_a can be computed by a linear regression between $\ln I_{\text{corr}}$ and $1/T$ (Figure 3).

It is concluded that in the absence of inhibitors, the value of E_a is 10.05 kJ mol⁻¹, while in the presence of SbW₉-Mn-SnR, the value of E_a reaches 27.85 kJ mol⁻¹. This indicates that the corrosion reaction process needs to overcome a higher energy barrier in the presence of inhibitors, which form an adsorption film covering the 20[#] carbon steel surface, thus slowing down the corrosion rate.¹¹ Moreover, the activation enthalpy (ΔH) and activation entropy (ΔS) were attained using the transition state equation (eq 5):⁹

$$\ln \frac{I_{\text{corr}}}{T} = \left(\ln \frac{R}{Nh} + \frac{\Delta S}{R} \right) - \frac{\Delta H}{RT} \quad (5)$$

where h is Planck's constant and N is Avogadro's number. Figure 4 shows the plot of $\ln I_{\text{corr}}/T$ vs $1/T$, from which the values of ΔS and ΔH have been calculated. All of the thermodynamic parameters are presented in Table 5.

It can be seen from Table 5 that the values of ΔS and ΔH in the inhibited system are significantly increased compared with those in the uninhibited system. The values of ΔH for both inhibited and uninhibited systems are positive, reflecting that the dissolution process of carbon steel is endothermic. The increase

Table 5. Thermodynamic Parameters for 20[#] Carbon Steel in the Presence and Absence of SbW₉-Mn-SnR in 0.5 M HCl Solution

	E_a (kJ mol ⁻¹)	ΔH (kJ mol ⁻¹)	ΔS (J mol ⁻¹ K ⁻¹)
blank	10.05	7.46	-276.32
SbW ₉ -Mn-SnR	27.85	25.26	-243.39

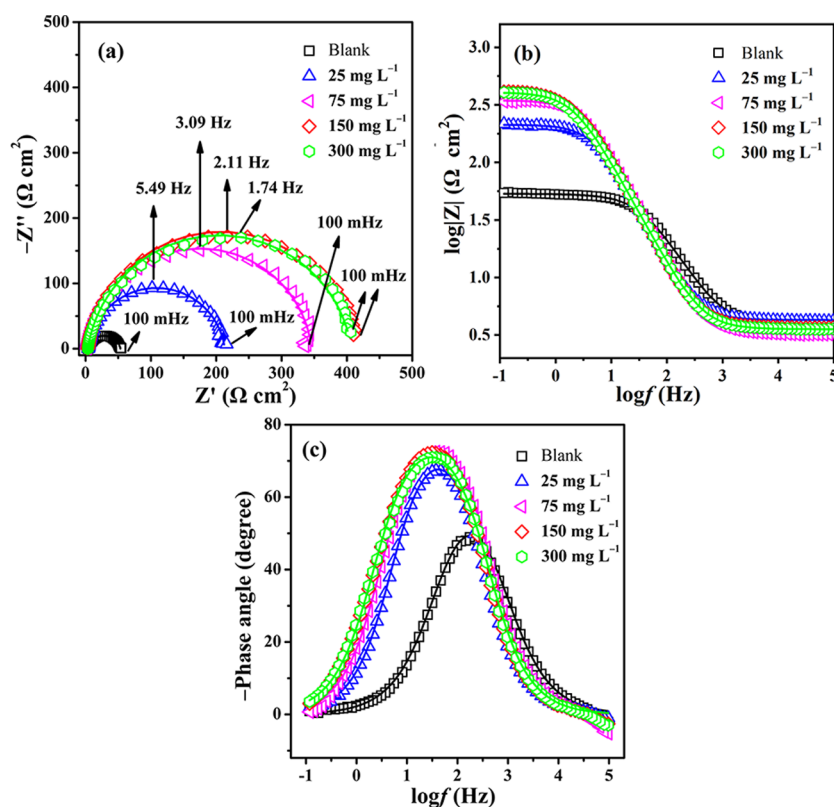


Figure 5. Nyquist plots (a), Bode modulus plots (b), and Bode phase plots (c) of 20[#] carbon steel immersed in 0.5 M HCl solution in the absence (blank) and presence of different concentrations (25, 75, 150, and 300 mg L⁻¹) of the SbW₉-Mn-SnR inhibitor at room temperature (the solid line shows fitted results).

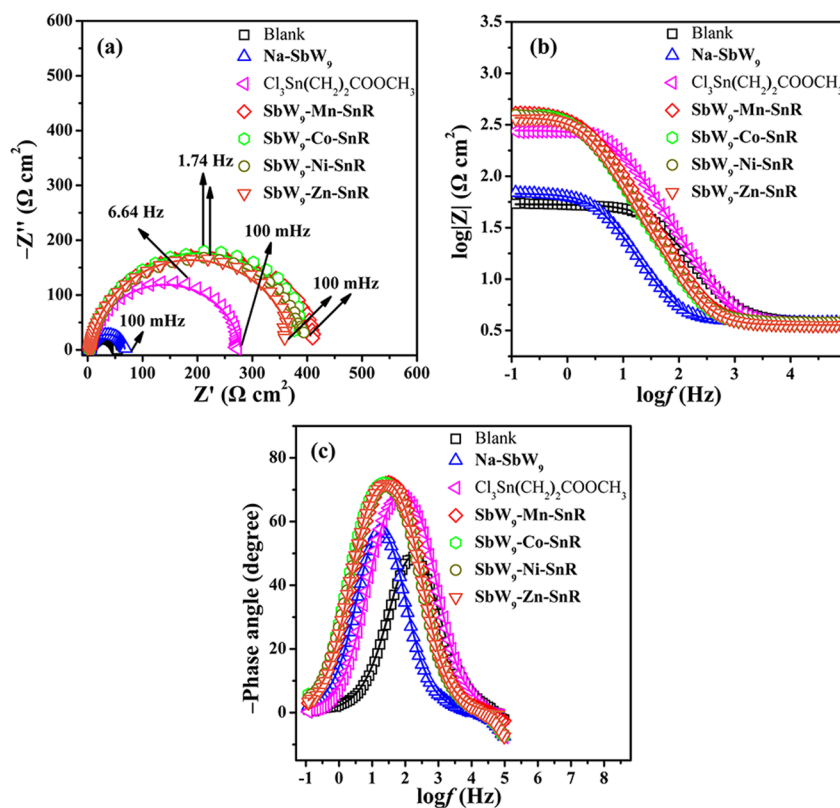


Figure 6. Nyquist plots (a), Bode modulus plots (b), and Bode phase plots (c) of 20[#] carbon steel immersed in 0.5 M HCl solution in the absence (blank) and presence of 150 mg L⁻¹ Na-SbW₉/Cl₃Sn(CH₂)₂COOCH₃/SbW₉-TM-SnR (TM = Mn, Co, Ni, and Zn) inhibitors at room temperature (the solid line shows fitted results).

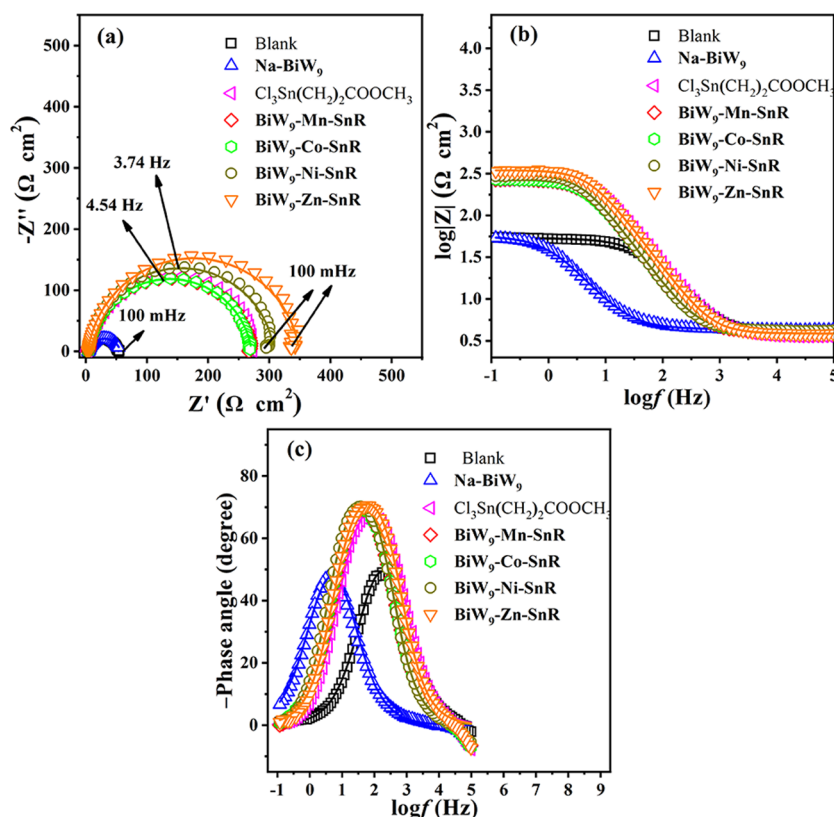


Figure 7. Nyquist plots (a), Bode modulus plots (b), and Bode phase plots (c) of 20[#] carbon steel immersed in 0.5 M HCl solution in the absence (blank) and presence of 150 mg L⁻¹ Na-BiW₉/Cl₃Sn(CH₂)₂COOCH₃/BiW₉-TM-SnR (TM = Mn, Co, Ni, and Zn) inhibitors at room temperature (the solid line shows fitted results).

in the ΔH value in the presence of SbW₉-Mn-SnR again proves that the energy barrier of the corrosion reaction is increased.⁴⁰ The value of ΔS in the presence of an inhibitor ($-243.39 \text{ J mol}^{-1} \text{ K}^{-1}$) is higher than that in blank solution ($-276.32 \text{ J mol}^{-1} \text{ K}^{-1}$), which is because the value of ΔS is the algebraic sum of the adsorption of inhibitors and desorption of water molecules.⁴¹

Electrochemical Impedance Spectroscopy (EIS) Analysis. EIS measurements were performed to study the corrosion behavior of 20[#] carbon steel in 0.5 M HCl solution at 298 K in the absence and presence of the POM-based inhibitors in the frequency range from 100 mHz to 100 kHz.⁴² Taking SbW₉-Mn-SnR for example, the Nyquist, Bode modulus, and phase plots for 20[#] carbon steel in 0.5 M HCl solution in the presence of various concentrations (0–300 mg L⁻¹) of SbW₉-Mn-SnR are shown in Figure 5. As seen from Figure 5a, the Nyquist graphic exhibits a depressed semicircle, which can be explained by the inhomogeneities and roughness of the carbon steel surface, and the semicircle diameter is related to the corrosion resistance of 20[#] carbon steel in 0.5 M HCl solution.⁴³ It is found that as the inhibitor concentration increases, the diameter of the arc gradually increases, indicating a better protection of the metal surface. Moreover, the Nyquist plots show a single capacitive loop, and the Bode plots exhibit only one peak attributed to one time constant for all samples, which indicates that the charge transfer process controls the corrosion reaction of carbon steel in HCl solution.⁴⁴ The impedance modulus is a measure of the protection against corrosion. The Bode modulus diagrams in Figure 5b show that the impedance modulus at the lowest frequency increases with the increase in the inhibitor concentration. Generally, the higher the impedance modulus at the lowest frequency, the higher the corrosion inhibition ability

of the sample.¹⁶ In addition, the increasing phase angle may be attributed to the improvement of uniformity, which is mainly due to the formation of an adsorption layer at the metal interface. A higher coverage results in a greater phase shift. As shown in the Bode phase plots in Figure 5c, the values of the phase angle are higher for carbon steel in 0.5 M HCl solution containing SbW₉-Mn-SnR than that in blank solution. The phase angle increases when the concentration of SbW₉-Mn-SnR increases and reaches the maximum ($\sim 74^\circ$) at 150 mg L⁻¹.

For comparison, at a concentration of 150 mg L⁻¹, the inhibition effect of SbW₉-TM-SnR/BiW₉-TM-SnR (TM = Mn, Co, Ni, and Zn), Na-SbW₉, Na-BiW₉, and Cl₃Sn-(CH₂)₂COOCH₃ on 20[#] carbon steel immersed in 0.5 M HCl solution at room temperature was also evaluated by the EIS plots (Figures 6 and 7). As evident from Figures 6a and 7a, the diameters of the semicircles in the presence of Cl₃Sn-(CH₂)₂COOCH₃ and SbW₉-TM-SnR/BiW₉-TM-SnR are larger than that of Na-SbW₉/Na-BiW₉, indicating that the corrosion behavior between the interface of the metal and HCl solution is prevented, and Cl₃Sn(CH₂)₂COOCH₃ and SbW₉-TM-SnR/BiW₉-TM-SnR have an obviously better corrosion inhibition property for carbon steel. For different inhibitors SbW₉-TM-SnR/BiW₉-TM-SnR containing SnR and different TMs, their corrosion inhibition effect on carbon steel is not obviously different, and this result is confirmed again by the Bode modulus and phase plots (Figures 6b,c and 7b,c). Therefore, SnR is a more important factor for improving the corrosion inhibition effect of these POM-esterin derivatives.

The impedance diagrams were analyzed using ZView 2 software in terms of the equivalent circuit (Figure 8), where R_s is the solution resistance, R_{ct} is the charge transfer resistance, and

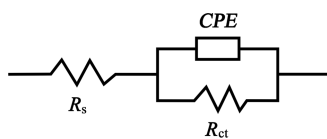


Figure 8. Equivalent circuit model used for fitting electrochemical impedance data.

CPE is the constant phase element. The inhibition efficiency (IE_R) was computed using eq 6:⁴⁵

$$IE_R(\%) = \left[1 - \frac{R_{ct}^o}{R_{ct}} \right] \times 100 \quad (6)$$

where R_{ct}^o and R_{ct} are charge transfer resistances without and with inhibitors, respectively.

Because the carbon steel/solution interface does not act as an ideal capacitor, the CPE is used to deal with nonideal capacitance response.^{43,46} The impedance of the CPE and the double-layer capacitance (C_{dl}) can be described using eqs 7 and 8,^{47,48} respectively.

$$Z_{CPE} = Y_0^{-1}(j\omega)^{-n} \quad (7)$$

$$C_{dl} = \frac{1}{2\pi f_{max} R_{ct}} \quad (8)$$

Y_0 is the CPE constant, j is the imaginary value ($j^2 = -1$), ω is the angular frequency (rad s^{-1}), and n is a phase shift, which represents a measure of surface inhomogeneity. When the value of n is 1, 0, and -1 , CPE represents the capacitance (C), resistance (R), and inductance (L), respectively. So, the value of n is an important parameter to show the surface character at the interface of carbon steel and acidic solution.⁴⁹ f_{max} is the frequency corresponding to the maximum value of the imaginary part in the impedance spectrum.

The corresponding impedance parameters were obtained by fitting the EIS plot using ZView 2 software and are listed in Table 6. It can be seen from the table that the λ^2 values lie between 0.0007 and 0.0081, indicating that the equivalent circuit and experimental data can be well-fitted.

Compared with the blank (0.5 M HCl solution), the values of R_{ct} gradually increase with the concentrations of inhibitors

increasing; moreover, the corrosion inhibition effect for **SbW₉-TM-SnR**/**BiW₉-TM-SnR** (TM = Mn, Co, Ni, and Zn) is obviously better than that of parent **Na-SbW₉**/**Na-BiW₉** and also better than those of some reported surfactant inhibitors.⁵⁰ The n values are also significant parameters to evaluate the surface property at the metal–acid interface. In the investigation, the values of n are within the range of 0.85 to 0.93, implying the inhomogeneity or roughness of the carbon steel surface, which causes the slight deviation from an ideal capacitance.^{35,48} These results again prove that **SbW₉-TM-SnR**/**BiW₉-TM-SnR** possess good corrosion inhibition behavior for 20[#] carbon steel in 0.5 M HCl solution.

The corrosion action of 20[#] carbon steel in 0.5 M HCl solution in the absence and presence of **SbW₉-Mn-SnR** at different immersion times (6, 10, 24, and 48 h) was also investigated by the EIS measurements at room temperature. The Nyquist, Bode modulus, and phase plots are shown in Figure S8, and the EIS parameters are listed in Table 7. It is found that the diameter of the semicircle increases at all immersion times in the presence of **SbW₉-Mn-SnR** compared to that in the blank (Figure S8a,d). The highest value of R_{ct} in the inhibitor-containing solution is achieved after 10 h of exposure (Table 7). Afterward, the extended immersion time (24 and 48 h) results in the decreased values of R_{ct} and n , indicating that the corrosion behavior recovers, which may be due to the increase in the number of microcracks in the adsorption film on the metal surface.

Adsorption Isotherm. In order to clarify the adsorption mechanism of these inhibitors on the surface of carbon steel in 0.5 M HCl solution, taking **SbW₉-Mn-SnR** for example, different adsorption models including Langmuir, Frumkin, Temkin, Freundlich, Flory–Huggins, and El-Awady isotherms were separately used to analyze the adsorption behaviors of POM-based inhibitors.^{7,40} It is found from Figure 9 that the experimental data could be well-fitted with the Langmuir adsorption isotherm with $R^2 > 0.99$. The other tested isotherms are shown in Figure S9. It is proven that **SbW₉-Mn-SnR** forms a monomolecular adsorption layer on the surface of 20[#] carbon steel, which prevents the corrosion behavior of metals. The Langmuir adsorption isotherm can be described using eq 9:⁵¹

Table 6. Electrochemical Impedance Spectroscopy Parameters for 20[#] Carbon Steel in 0.5 M HCl in the Absence (Blank) and Presence of Inhibitors at Room Temperature (298 K)

inhibitor	inhibitor concentration (mg L ⁻¹)	R_s (Ω cm ²)	R_{ct} (Ω cm ²)	C_{dl} (μ F cm ⁻²)	Y_0 (μ F cm ⁻²)	λ^2	n	IE_R (%)
blank		3.8	49.6	85.3	182.0	0.0015	0.86	
SbW₉-Mn-SnR	25	4.3	208.7	138.9	193.8	0.0007	0.93	76.2
	75	3.2	342.8	150.3	183.3	0.0023	0.93	85.5
	150	3.7	407.2	185.3	212.7	0.0014	0.92	87.8
	300	3.6	403.6	226.6	229.2	0.0020	0.91	87.7
	SbW₉-Co-SnR	150	3.6	398.8	229.4	261.2	0.0036	0.92
SbW₉-Ni-SnR	150	3.8	390.0	234.5	265.7	0.0031	0.91	87.3
SbW₉-Zn-SnR	150	3.6	370.5	246.9	247.4	0.0034	0.92	86.6
BiW₉-Mn-SnR	150	4.0	265.2	132.2	64.1	0.0029	0.93	81.0
BiW₉-Co-SnR	150	4.1	265.5	132.0	168.9	0.0032	0.93	81.1
BiW₉-Ni-SnR	150	4.2	297.7	142.9	164.2	0.0028	0.93	83.1
BiW₉-Zn-SnR	150	3.9	343.6	84.4	113.2	0.0038	0.92	85.4
Na-SbW₉	150	3.8	64.0	664.9	828.7	0.0051	0.92	22.5
Na-BiW₉	150	4.3	52.6	2564.2	3746.0	0.0081	0.85	4.5
Cl₃Sn(CH₂)₂COOCH₃	150	3.6	275.6	71.6	109.7	0.0041	0.91	82.0

Table 7. EIS Parameters for 20[#] Carbon Steel in 0.5 M HCl in the Absence (Blank) and Presence of Inhibitors at Room Temperature (298 K)

inhibitor	time (h)	R_s (Ω cm ²)	R_{ct} (Ω cm ²)	C_{dl} (μ F cm ⁻²)	CPE-T (μ F cm ⁻²)	n	IE _R (%)
blank	6	3.41	39.29	340.12	596.78	0.88487	
	10	3.323	15.37	1283.0	2071.2	0.86419	
	24	3.951	39.02	614.02	1084.1	0.86987	
	48	4.266	34.23	1242.57	1799.6	0.8795	
SbW ₉ -Mn-SnR	6	3.168	389.1	615.75	705.64	0.92858	89.9
	10	2.14	495.6	1259.39	1337	0.93404	96.9
	24	3.098	339.8	3956.01	4093.6	0.91716	88.5
	48	4.114	139.3	11699.44	11298.0	0.83694	75.4

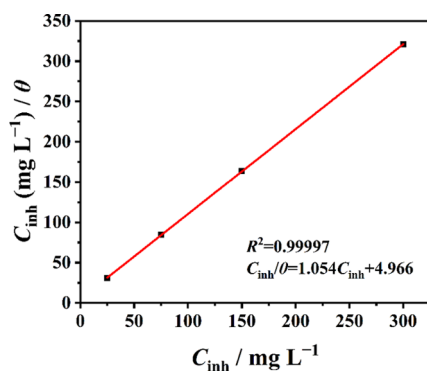


Figure 9. Langmuir adsorption isotherm of SbW₉-Mn-SnR on 20[#] carbon steel in 0.5 M HCl solution at 298 K.

$$\frac{C_{inh}}{\theta} = C_{inh} + \frac{1}{K_{ads}} \quad (9)$$

C_{inh} is the inhibitor concentration, θ is the surface coverage ($\theta = IE/100$), and K_{ads} is the adsorption/desorption equilibrium constant.

The K_{ads} value can be calculated from the intercept of the line on the C_{inh}/θ axis. Accordingly, the standard free energy (ΔG_{ads}^0) can be obtained from the following equation (eq 10):⁵²

$$\Delta G_{ads}^0 = -RT \ln(55.5K_{ads}) \quad (10)$$

in which T is the thermodynamic temperature (298 K), R (8.314 J mol⁻¹ K⁻¹) is the gas constant, and 55.5 (M) is the molar concentration of water in the solution. In this case, the calculated

values of K_{ads} and ΔG_{ads}^0 are 1156.06 L mol⁻¹ and -27.43 kJ mol⁻¹, respectively. The high value of K_{ads} indicates that SbW₉-Mn-SnR is robustly adsorbed on the 20[#] carbon steel surface. It is generally acknowledged that the negative value of ΔG_{ads}^0 shows that the formation of the above POM-based protective film on the metal surface is a spontaneous adsorption process. According to the literature,^{30,53} when $\Delta G_{ads}^0 > -20$ kJ mol⁻¹, the adsorption of the inhibitor on the metal surface can be considered as physical adsorption; if -40 kJ mol⁻¹ < ΔG_{ads}^0 < -20 kJ mol⁻¹, then the interaction between inhibitor molecules and metal atoms can be attributed to physical adsorption and chemical adsorption. Hence, the ΔG_{ads}^0 of -27.43 kJ mol⁻¹ for this paper suggests that physical and chemical adsorption has taken place between SbW₉-Mn-SnR and 20[#] carbon steel, but it is mainly physical adsorption.

Surface Morphology and Composition of 20[#] Carbon Steel. The surface morphology of 20[#] carbon steel after corrosion testing was observed by SEM (Figure 10). As expected, it can be seen from Figure 10a,b that severe corrosive attack occurred on the surface of carbon steel in 0.5 M HCl solution without the inhibitor and with the raw material Na-SbW₉, respectively. Conversely, the damage degree of carbon steel in 0.5 M HCl solution with SbW₉-TM-SnR (TM = Mn, Co, Ni, and Zn) inhibitors (Figure 10c–f) is weaker, and the surfaces are smoother. This phenomenon further indicates that these sandwich-type POMs modified by SnR and TMs can be used as good corrosion inhibitors to protect carbon steel well in 0.5 M HCl solution. Figure 11a,b shows EDX diagrams for 20[#] carbon steel immersed in 0.5 M HCl solution containing no

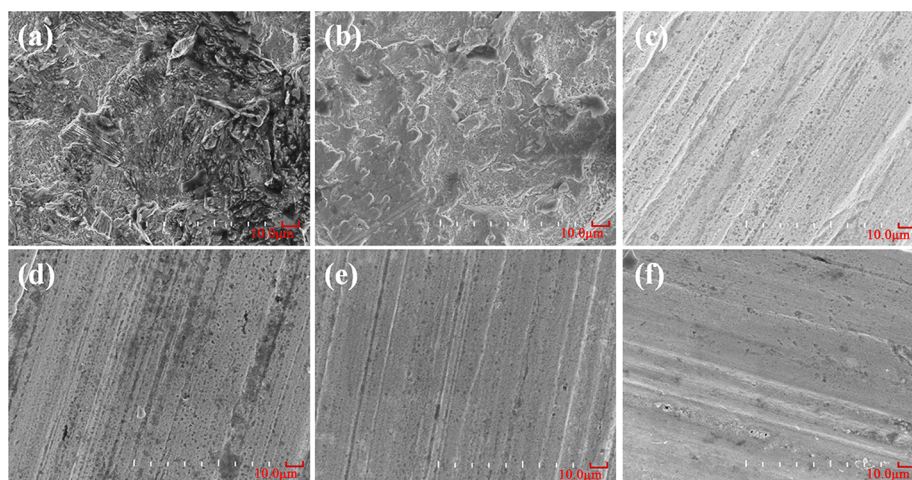


Figure 10. SEM images of the carbon steel surface after 6 h of immersion in 0.5 M HCl solution without an inhibitor (a) and with Na-SbW₉ (b) and SbW₉-TM-SnR (TM = Mn, Co, Ni, and Zn) (c–f).

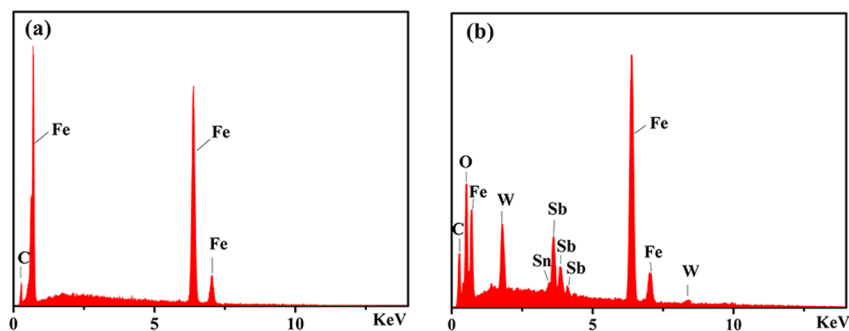


Figure 11. EDX analysis of carbon steel immersed in 0.5 M HCl solution without an inhibitor (a) and with the $\text{SbW}_9\text{-Mn-SnR}$ inhibitor (b).

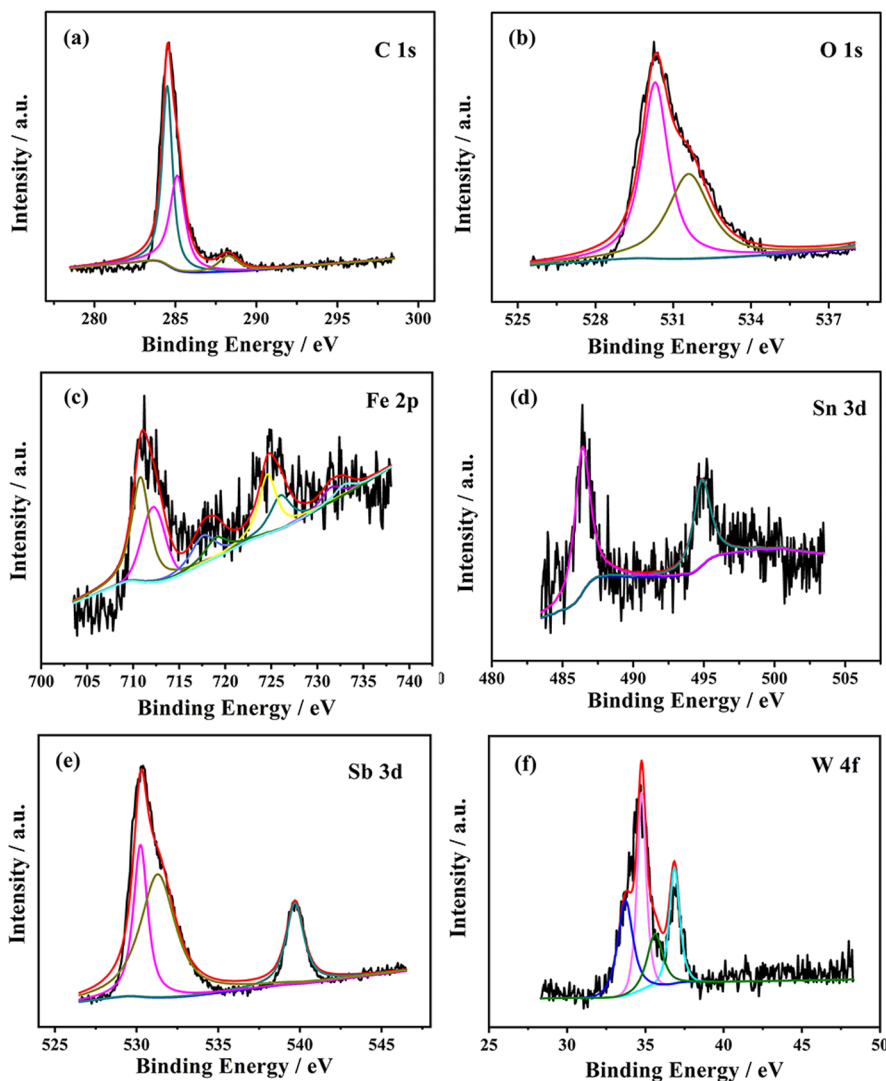


Figure 12. XPS analysis of C 1s, O 1s, Fe 2p, Sn 3d, Sb 3d, and W 4f (a–f) on the 20[#] carbon steel surface after immersion in 0.5 M HCl solution containing $\text{SbW}_9\text{-Mn-SnR}$ for 6 h.

inhibitor and the inhibitor $\text{SbW}_9\text{-Mn-SnR}$, respectively. Compared with Figure 11a, Figure 11b exhibits the existence of O, W, Sb, and Sn in addition to C and Fe elements on the film surface of carbon steel; the result proves that the POM-based corrosion inhibitor exists on the carbon steel surface. However, no Mn was detected in the EDX spectrum, which may be caused by the following reasons: (1) the content of TM is relatively low; (2) two TM ions are located at the active sites on both sides of the intermediate belt in the sandwich-type structures, so they are

easily replaced by the formed $\text{Fe}^{2+}/\text{Fe}^{3+}$ ions, forming a protective film on the carbon steel surface. This substitution reaction also often occurred in other sandwich-type POMs.^{54–56}

In order to characterize the oxidation states of various elements existing on the carbon steel surface, taking $\text{SbW}_9\text{-Mn-SnR}$ as an example, XPS analysis of 20[#] carbon steel after immersion in 0.5 M HCl containing 150 mg L^{-1} $\text{SbW}_9\text{-Mn-SnR}$ for 6 h was performed (Figure 12). The signal of Mn was not detected because of its low content. As shown in Figure 12a, XPS

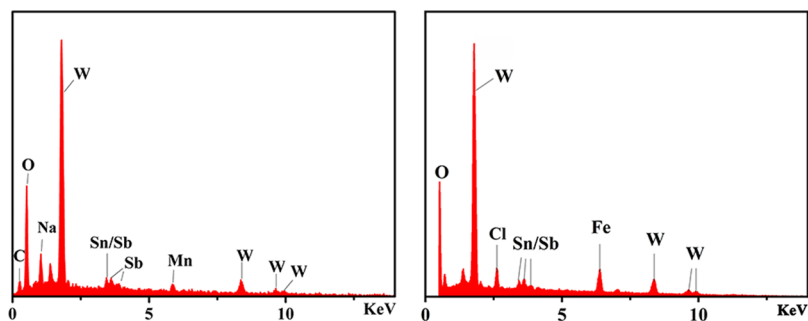


Figure 13. EDX analysis of pure $\text{SbW}_9\text{-Mn-SnR}$ (left) and a solid sample obtained by recrystallization for several times in 0.5 M HCl solution containing 150 mg L^{-1} $\text{SbW}_9\text{-Mn-SnR}$ and Fe powder (right).

peaks of C 1s can be fitted with three peaks at binding energies of 284.5, 285.12, and 288.27 eV, which are ascribed to C–C/C–H species, C–O, and C=O/O–C=O bonds in SnR groups, respectively.⁵⁷ As seen from Figure 12b, O 1s shows signals at binding energies of 530.3 and 531.6 eV, which correspond to O^{2-} and OH^- , respectively.^{58,59} As for Fe 2p, in Figure 12c, the peak positions of Fe $2p_{1/2}$ and Fe $2p_{3/2}$ for Fe^{2+} are located at 724.6 and 710.8 eV, with their associated satellite peaks at 731.5 and 717.6 eV, respectively. In addition, the XPS peaks with binding energies of 726 and 712.2 eV are assigned to Fe $2p_{1/2}$ and Fe $2p_{3/2}$ for Fe^{3+} , with their associated satellite peaks at 732.9 and 719 eV, respectively. The above test results show that Fe^{2+} and Fe^{3+} oxide films are formed on the surface of carbon steel.⁶⁰ In Figure 12d, the binding energies of Sn 3d located at 486.4 and 494.85 eV are attributed to the Sn^{4+} oxidation state.⁵⁸ Figure 12e shows the XPS spectra of Sb 3d, in which the peaks at binding energies of 539.7 and 530.24 eV are ascribed to Sb $3d_{3/2}$ and Sb $3d_{5/2}$ for the Sb^{3+} oxidation state, in which there exists an overlap between the O 1s peak at 531.3 eV and the Sb $3d_{5/2}$ peak.^{32,61} In Figure 12f, the peaks at binding energies of 36.9 and 34.8 eV are attributed to W $4f_{7/2}$ and W $4f_{5/2}$ for the W^{6+} oxidation state, and the peaks at binding energies of 35.7 and 33.7 eV are assigned to W $4f_{7/2}$ and W $4f_{5/2}$ for the W^{5+} oxidation state, respectively, inferring that part of the W element in POM is reduced in the HCl media.^{32,62}

Stability Analysis of Corrosion Inhibitors. The stability of inhibitors in the corrosion test was studied by IR and UV–vis absorption spectra. To evaluate the stability of these POMs after the corrosion tests, iron powder was used instead of the carbon steel plate to simulate the corrosion test. Taking $\text{SbW}_9\text{-Mn-SnR}$ for example, the IR spectra of the solid samples recrystallized from the following HCl solutions were tested (Figure S10): (1) 150 mg L^{-1} $\text{SbW}_9\text{-Mn-SnR}$ in 0.5 M HCl solution and excessive Fe powder, 6 h (curve a); (2) 150 mg L^{-1} $\text{SbW}_9\text{-Mn-SnR}$ in 0.5 M HCl solution and no Fe powder, 6 h (curve b). As seen from curves a and b in Figure S10, the main peaks appearing at 2950–2800, 1650, and 1000–600 cm^{-1} are the characteristic peaks of CH_2 , COO, and POM, respectively,³⁰ which is consistent with that of the pure original $\text{SbW}_9\text{-Mn-SnR}$ (curve c). This result proves that the skeleton of the POM is still stable in the acidic solution. In addition, UV–vis absorption spectra of $\text{SbW}_9\text{-Mn-SnR}$ dissolved in 0.5 M HCl solution for 0 and 6 h (curves a and b in Figure S11), and with adding Fe powder (curve c in Figure S11) for 6 h, were recorded to identify the inhibitor stability. As shown in Figure S11, two peaks in the UV region of 200–300 nm attributed to $\text{O} \rightarrow \text{W}$ charge transfer transitions are observed in curve a and unchanged in curves b and c. In order to further evaluate the stability of corrosion inhibitors in more acidic

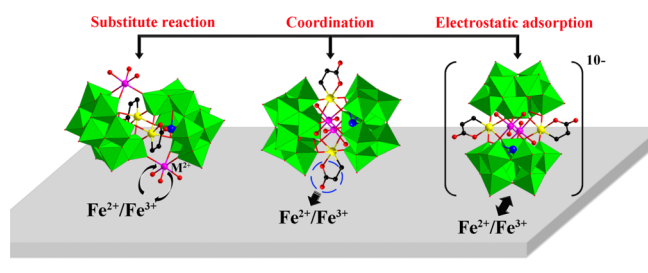
solutions, similar experiments were carried out in 1.0 and 2.0 M HCl solutions, respectively. As can be seen from Figures S12 and S13, the characteristic peaks of IR and UV–vis absorption spectra are consistent with Figures S10 and S11, which indicate that the POM skeleton still exists in 1.0–2.0 M HCl media. However, the ^{119}Sn NMR spectrum (Figure S14) shows that the inhibitor breaks down in 2.0 M HCl because the signal ($\delta = -424.06 \text{ ppm}$) is similar to that of pure SnR ($\delta = -416.84 \text{ ppm}$). This verifies the above speculation that the IE_w of the corrosion inhibitor in 2 M HCl is lower than that in 1 M HCl because of decomposition of anionic POM. To sum up, these sandwich-type POM-based corrosion inhibitors containing SnR and TMs remain stable in 0.5–1.0 M HCl solutions.

Corrosion Inhibition Mechanism. In order to further explore the film-forming mechanism, EDX analysis (Figure 13) was also carried out on the above described $\text{SbW}_9\text{-Mn-SnR}$ recrystallized from HCl solution treated with Fe powder. Compared with the pure original $\text{SbW}_9\text{-Mn-SnR}$ (Figure 13a), the Mn content of the solid sample recrystallized from 0.5 M HCl solution illustrated in Figure 13b is actually reduced, and other elements have not changed significantly. Importantly, the appearance of the Fe signal peak further confirms the conjecture that the Fe^0 on the surface of carbon steel is oxidized to $\text{Fe}^{2+}/\text{Fe}^{3+}$ in HCl solution, and the formed $\text{Fe}^{2+}/\text{Fe}^{3+}$ further replaces TM ions situated on either side of the middle part in $\text{SbW}_9\text{-TM-SnR}/\text{BiW}_9\text{-TM-SnR}$ (TM = Mn, Co, Ni, and Zn), thereby preventing further corrosion of Fe in the carbon steel. In addition, $\text{Fe}^{2+}/\text{Fe}^{3+}$ on the carbon steel surface possesses two/three positive charges in HCl solution, while $[(\text{TM}(\text{H}_2\text{O})_3)_2(\text{SnCH}_2\text{CH}_2\text{COO})_2(\text{SbW}_9\text{O}_{33})_2]^{10-}/[(\text{TM}(\text{H}_2\text{O})_3)_2(\text{SnCH}_2\text{CH}_2\text{COO})_2(\text{BiW}_9\text{O}_{33})_2]^{10-}$ in $\text{SbW}_9\text{-TM-SnR}/\text{BiW}_9\text{-TM-SnR}$ is a large polyoxoanion cluster with 10 negative charges, so the POMs can be easily adsorbed on the surface of carbon steel by electrostatic adsorption. Furthermore, the exposed COO group of SnR in the POM corrosion inhibitor can provide lone electron pairs to interact with the empty 3d orbital of Fe atoms, forming the coordination covalent bond,⁶³ which resulted in a denser protective film on the surface of carbon steel through chemical and physical adsorption. Consequently, the combined actions of physical adsorption and chemical adsorption delay the corrosion of carbon steel (Scheme 1).

CONCLUSIONS

This work first reports the inhibition behaviors of $\text{SbW}_9\text{-TM-SnR}$ and $\text{BiW}_9\text{-TM-SnR}$ (TM = Mn, Co, Ni, and Zn) in a HCl medium. The inhibition performance of the lacunary POMs is greatly improved by carboxyethyltin functionalization. The

Scheme 1. Schematic Diagram of the Corrosion Inhibition Mechanism of $\text{SbW}_9\text{-TM-SnR}$ / $\text{BiW}_9\text{-TM-SnR}$ (TM = Mn, Co, Ni, and Zn) on $20^\#$ Carbon Steel in the HCl Solution



inhibition efficiency of $\text{SbW}_9\text{-TM-SnR}$ is slightly higher than that of $\text{BiW}_9\text{-TM-SnR}$. The electrochemical and surface analyses show that $\text{SbW}_9\text{-TM-SnR}$ and $\text{BiW}_9\text{-TM-SnR}$ act as mixed-type inhibitors, forming stable and protective films on the surface of carbon steel by physical and chemical adsorption. The adsorption process follows the Langmuir adsorption isotherm. This work also shows the high acid resistance of the sandwich-type POM-estertin derivatives with Sb/Bi as a heteroatom for the first time.

MATERIALS AND EXPERIMENTAL METHODS

Materials. All chemicals and reagents (analytical grade) were commercially available. $\text{Na}_9[\text{B-}\alpha\text{-SbW}_9\text{O}_{33}] \cdot 19.5\text{H}_2\text{O}$ (Na-SbW_9), $\text{Na}_9[\text{B-}\alpha\text{-BiW}_9\text{O}_{33}] \cdot 16\text{H}_2\text{O}$ (Na-BiW_9), and $\text{Cl}_3\text{Sn}(\text{CH}_2)_2\text{COOCH}_3$ were synthesized according to the reported procedures.^{64–66} HCl solution (0.5 M) was prepared by diluting 37% HCl solution with water. All tests were performed at room temperature, and the water used in all experiments was secondary distilled water.

Weight Loss Measurement. The new $20^\#$ carbon steel plates (the size is 4 cm \times 1 cm \times 0.2 cm with the compositions of C, 0.23; Si, 0.29; Mn, 0.60; and S, 0.028 in wt % and Fe in balance) were washed with acetone and ethanol and then dried in a desiccator for more than 24 h to a constant weight before immersion in the test solutions. The specific test procedures used in weight loss measurement were as follows: the carbon steel plates were immersed in 0.5, 1.0, and 2.0 M HCl solutions containing different corrosion inhibitors. The concentrations of corrosion inhibitors were 25–500 mg L^{-1} , and the corrosion test time at room temperature was 6 and 10 h, respectively. After the steel specimen was taken out from HCl solutions, its surface was cleaned with water and ethanol and then dried for more than 24 h to a constant weight. Three sets of parallel experiments were performed for each test to ensure the accuracy of the experiment.

Electrochemical Measurements. Electrochemical measurements were conducted in a three-electrode system on a CHI604B electrochemical workstation by using a platinum plate (20 mm \times 60 mm \times 0.1 mm) as the counter electrode, a saturated calomel electrode (SCE) as the reference electrode, and a $20^\#$ carbon steel sample with an exposed area of 1 cm^2 as the working electrode. To reach a steady state, the working electrode should be immersed in the measured solution for 1 h before the measurement. As for polarization tests, the Tafel curve was obtained in the potential range from -0.5 to 0.1 V, and the scan rate was 1 mV s^{-1} . The corrosion potential (E_{corr}) and corrosion current density (I_{corr}) were obtained by Tafel extrapolation of anode and cathode polarization curves. The electrochemical impedance test was performed with an AC amplitude of 5 mV at the corrosion potential and a frequency

range of 100 mHz to 100 kHz; all impedance data were fitted to the relevant impedance parameters by ZView 2 software.

Surface Analysis. The morphology and composition of the surfaces of $20^\#$ carbon steel samples in 0.5 M HCl without and with different inhibitors were investigated by a HITACHI SU8010 serious microscope equipped with EDX after weight loss tests. X-ray photoelectron spectroscopy (XPS) analysis was performed on an ESCALAB-MKII X-ray spectrometer with a Mg $K\alpha$ (1253.6 eV) X-ray source.

Corrosion Inhibitor Stability Analysis. Taking $\text{SbW}_9\text{-Mn-SnR}$ as a sample, the stability of the corrosion inhibitor was analyzed by IR and UV spectroscopy. The FT-IR spectra were measured on a Bruker AXS TENSOR-27 spectrometer using KBr pellets at 4000–400 cm^{-1} . Using a PerkinElmer Lambda 35 spectrometer with a wavelength range of 200–800 nm, the UV–vis absorption spectra of $\text{SbW}_9\text{-Mn-SnR}$ solutions were obtained. NMR spectra were recorded at room temperature on a 500 MHz Bruker AVANCE 500 spectrometer. An inner tube containing D_2O was used as an instrumental lock. Tin chemical shifts were referenced to $\text{Cl}_3\text{Sn}(\text{CH}_2)_2\text{COOCH}_3$.

ASSOCIATED CONTENT

Supporting Information

The Supporting Information is available free of charge at <https://pubs.acs.org/doi/10.1021/acsomega.1c06276>.

Synthesis, characterization, corrosion inhibition performance, adsorption isotherm, and stability analysis of corrosion inhibitors (PDF)

Crystallographic information on $\text{BiW}_9\text{-Ni-SnR}$ (CIF)

Crystallographic information on $\text{BiW}_9\text{-Zn-SnR}$ (CIF)

AUTHOR INFORMATION

Corresponding Authors

Zai-Ming Zhu – School of Chemistry and Chemical Engineering, Liaoning Normal University, Dalian 116029, P. R. China; Phone: +86 0411 82159780; Email: chemzhu@sina.com

Xiao-Jing Sang – School of Chemistry and Chemical Engineering, Liaoning Normal University, Dalian 116029, P. R. China; Phone: +86 0411 82159780; Email: sangxj923@lnnu.edu.cn

Lan-Cui Zhang – School of Chemistry and Chemical Engineering, Liaoning Normal University, Dalian 116029, P. R. China; orcid.org/0000-0001-6352-9292; Phone: +86 0411 82159780; Email: zhanglancui@lnnu.edu.cn

Authors

Xing-Fang Wang – School of Chemistry and Chemical Engineering, Liaoning Normal University, Dalian 116029, P. R. China

Xin-Yu Liu – School of Chemistry and Chemical Engineering, Liaoning Normal University, Dalian 116029, P. R. China

Fang Su – School of Chemistry and Chemical Engineering, Liaoning Normal University, Dalian 116029, P. R. China

Jian-Sheng Li – School of Chemistry and Chemical Engineering, Liaoning Normal University, Dalian 116029, P. R. China; orcid.org/0000-0001-7105-6149

Complete contact information is available at <https://pubs.acs.org/doi/10.1021/acsomega.1c06276>

Author Contributions

[#]X.-F.W. and X.-Y.L. contributed equally to this work and should be considered as co-first authors.

Notes

The authors declare no competing financial interest.

ACKNOWLEDGMENTS

This work was supported by the National Natural Science Foundation of China (nos. 21671091 and 21601077), the Natural Science Foundation of Liaoning Province (no. 20180550544), the Scientific Research Project of the Liaoning Normal University (GD19L005), and the High-Level Talent Innovation Support Program of Dalian (nos. 2020RQ046 and 2019RQ133).

REFERENCES

- (1) Yang, Y.; Cheng, Y. F. Visible light illuminated high-performance $\text{WO}_3\text{-TiO}_2\text{-BiVO}_4$ nanocomposite photoanodes capable of energy self-storage for photo-induced cathodic protection. *Corros. Sci.* **2020**, *164*, 108333.
- (2) Dandia, A.; Gupta, S. L.; Singh, P.; Quraishi, M. A. Ultrasound assisted synthesis of pyrazolo(3,4-*b*) pyridines as potential corrosion inhibitors for mild steel in 1.0 M HCl. *ACS Sustainable Chem. Eng.* **2013**, *1*, 1303–1310.
- (3) Ye, Y.; Yang, D.; Chen, H.; Guo, S.; Yang, Q.; Chen, L.; Zhao, H.; Wang, L. A high-efficiency corrosion inhibitor of N-doped citric acid-based carbon dots for mild steel in hydrochloric acid environment. *J. Hazard. Mater.* **2020**, *381*, 121019.
- (4) Bastos, A. C.; Ferreira, M. G.; Simões, A. M. Corrosion inhibition by chromate and phosphate extracts for iron substrates studied by EIS and SVET. *Corros. Sci.* **2006**, *48*, 1500–1512.
- (5) Alentejano, C. R.; Aoki, I. V. Localized corrosion inhibition of 304 stainless steel in pure water by oxyanions tungstate and molybdate. *Electrochim. Acta* **2004**, *49*, 2779–2785.
- (6) Goyal, M.; Kumar, S.; Bahadur, I.; Verma, C.; Ebenso, E. E. Organic corrosion inhibitors for industrial cleaning of ferrous and non-ferrous metals in acidic solutions: A review. *J. Mol. Liq.* **2018**, *256*, 565–573.
- (7) Aslam, R.; Mobin, M.; Huda; Shoeb, M.; Murmu, M.; Banerjee, P. Proline nitrate ionic liquid as high temperature acid corrosion inhibitor for mild steel: Experimental and molecular-level insights. *J. Ind. Eng. Chem.* **2021**, *100*, 333–350.
- (8) San, Y.; Sun, J.; Wang, H.; Jin, Z. H.; Gao, H. J. Synthesis of 1,8-naphthyridines by the ionic liquid-catalyzed friedlander reaction and application in corrosion inhibition. *ACS Omega* **2021**, *6*, 28063–28071.
- (9) Khanra, A.; Srivastava, M.; Rai, M. P.; Prakash, R. Application of unsaturated fatty acid molecules derived from microalgae toward mild steel corrosion inhibition in HCl solution: a novel approach for metal-inhibitor association. *ACS Omega* **2018**, *3*, 12369–12382.
- (10) Ngouné, B.; Pengou, M.; Nouteza, A. M.; Nansu-Njilki, C. P.; Ngameni, E. Performances of alkaloid extract from *rauvolfia macrophylla* stapf toward corrosion inhibition of C38 steel in acidic media. *ACS Omega* **2019**, *4*, 9081–9091.
- (11) Raghavendra, N.; Bhat, J. I. Natural products for material protection: an interesting and efficacious anticorrosive property of dry arecanut seed extract at electrode (aluminum)–electrolyte (hydrochloric acid) interface. *J. Bio. Tribo Corros.* **2016**, *2*, 21.
- (12) Wang, Y. N.; Dong, C. F.; Zhang, D. W.; Ren, P. P.; Li, L.; Li, X. G. Preparation and characterization of a chitosan-based low-pH-sensitive intelligent corrosion inhibitor. *Int. J. Min. Met. Mater.* **2015**, *22*, 998–1004.
- (13) Zhang, F.; Ju, P.; Pan, M.; Zhang, D.; Huang, Y.; Li, G.; Li, X. Self-healing mechanisms in smart protective coatings: a review. *Corros. Sci.* **2018**, *144*, 74–88.
- (14) Wang, J.; Tang, J.; Zhang, H.; Wang, Y.; Wang, H.; Lin, B.; Hou, J.; Zhang, H. A CO_2 -responsive anti-corrosion ethyl cellulose coating based on the pH-response mechanism. *Corros. Sci.* **2021**, *180*, 109194.
- (15) Attaei, M.; Calado, L. M.; Morozov, Y.; Taryba, M. G.; Shakoar, R. A.; Kahraman, R.; Marques, A. C.; Montemor, M. F. Smart epoxy coating modified with isophorone diisocyanate microcapsules and cerium organophosphate for multilevel corrosion protection of carbon steel. *Prog. Org. Coat.* **2020**, *147*, 105864.
- (16) Zang, Y.; Ramezanzadeh, B. Synthesis and characterization of a high-quality nanocontainer based on benzimidazole-zinc phosphate (ZP-BIM) tailored graphene oxides; A facile approach to fabricating a smart self-healing anti-corrosion system. *J. Colloid. Interface Sci.* **2020**, *564*, 230–244.
- (17) Katsoulis, D. E. A Survey of applications of polyoxometalates. *Chem. Rev.* **1998**, *98*, 359–388.
- (18) Zhang, Y.; Liu, J.; Li, S. L.; Su, Z. M.; Lan, Y. Q. Polyoxometalate-based materials for sustainable and clean energy conversion and storage. *EnergyChem.* **2019**, *1*, 100021.
- (19) Sruthi, G.; Shakeela, K.; Shanmugam, R.; Rao, G. R. Corrosion inhibition of stainless steel by ferrocene-polyoxometalate hybrid molecular materials-experimental and first principle studies. *Phys. Chem. Chem. Phys.* **2020**, *22*, 3329–3344.
- (20) Lomakina, S. V.; Shatova, T. S.; Kazansky, L. P. Heteropoly anions as corrosion inhibitors for aluminium in high temperature water. *Corros. Sci.* **1994**, *36*, 1645–1651.
- (21) Liang, C. H.; Hu, X. Q.; Ma, L. Effects of $\text{Na}_3\text{PW}_{12}\text{O}_{40}$ on the corrosion behavior of carbon steel in 55% LiBr solution. *Mater. Corros.* **2007**, *58*, 39–43.
- (22) Hu, X. Q.; Liang, C. H.; Wu, X. N. Corrosion behaviors of carbon steel in 55% LiBr solution containing PWVA inhibitor. *Mater. Corros.* **2011**, *62*, 444–448.
- (23) Ait Albrimi, Y.; Ait Addi, A.; Douch, J.; Souto, R. M.; Hamdani, M. Inhibition of the pitting corrosion of 304 stainless steel in 0.5 M hydrochloric acid solution by heptamolybdate ions. *Corros. Sci.* **2015**, *90*, 522–528.
- (24) Bonastre, J.; Garcés, P.; Huerta, F.; Quijada, C.; Andión, L. G.; Cases, F. Electrochemical study of polypyrrole/ $\text{PW}_{12}\text{O}_{40}^{3-}$ coatings on carbon steel electrodes as protection against corrosion in chloride aqueous solutions. *Corros. Sci.* **2006**, *48*, 1122–1136.
- (25) Herrmann, S.; Kostrzewa, M.; Wierschem, A.; Streb, C. Polyoxometalate Ionic Liquids as Self-Repairing Acid-Resistant Corrosion Protection. *Angew. Chem., Int. Ed.* **2014**, *53*, 13596–13599.
- (26) Al-Dawsari, A.; Turkustani, A. M.; Bannani, F. Acid-resistant corrosion protection polyoxometalate ionic liquids as anticorrosion coatings. *J. Mater. Environ. Sci.* **2019**, *10*, 1135–1151. ISSN 2028-2508
- (27) Misra, A.; Franco Castillo, I.; Müller, D. P.; Gonzalez, C.; Eyssautier-Chuine, S.; Ziegler, A.; de la Fuente, J. M.; Mitchell, S. G.; Streb, C. Polyoxometalate-Ionic Liquids (POM-ILs) as Anticorrosion and Antibacterial Coatings for Natural Stones. *Angew. Chem., Int. Ed.* **2018**, *57*, 14926–14931.
- (28) Mourad, M. Y.; Seliman, S. A.; Ibrahim, E. H. The inhibitive action of dimethyltin dichloride towards the corrosion of aluminium in hydrochloric acid and sodium hydroxide solutions. *J. Chem. Technol. Biotechnol.* **1989**, *46*, 27–40.
- (29) Zhang, L. C.; Zheng, S. L.; Xue, H.; Zhu, Z. M.; You, W. S.; Li, Y. G.; Wang, E. B. New tetra(organotin)-decorated boat-like polyoxometalate. *Dalton Trans.* **2010**, *39*, 3369–3371.
- (30) Wang, Z. X.; Sang, X. J.; Yang, H.; Ji, L. P.; Zhang, L. C.; Zhu, Z. M.; You, W. S. A new carboxyethyltin functionalized sandwich-type tungstoarsenate: Synthesis, catalytic activity and corrosion inhibition behavior for carbon steel. *Inorg. Chem. Commun.* **2017**, *83*, 44–48.
- (31) Sang, X. J.; Wang, Z. X.; Li, J. S.; Wang, H. D.; Su, F.; Liu, Z. B.; Zhang, L. C.; Zhu, Z. M. Corrosion protection of carbon steel in circulating cooling water by open-chain carboxyethyltin and transition metal co-functionalized tungstogermanates. *ChemistrySelect* **2018**, *3*, 7358–7362.
- (32) Wang, H. D.; Wang, X. F.; Su, F.; Li, J. S.; Zhang, L. C.; Sang, X. J.; Zhu, Z. M. Carboxyethyltin and transition metal co-functionalized tungstoantimonates composited with polypyrrole for enhanced electrocatalytic methanol oxidation. *Dalton Trans.* **2019**, *48*, 2977–2987.
- (33) Wang, Z. J.; Zhang, L. C.; Zhu, Z. M.; Chen, W. L.; You, W. S.; Wang, E. B. Two new sandwich-type tungstobismuthates constructed from trivalent Keggin units, estertin and transition metals. *Inorg. Chem. Commun.* **2012**, *17*, 151–154.

- (34) Loganayagi, C.; Kamal, C.; Sethuraman, M. G. Opuntiol: An Active Principle of Opuntia elatior as an Eco-Friendly Inhibitor of Corrosion of Mild Steel in Acid Medium. *ACS Sustainable Chem. Eng.* **2014**, *2*, 606–613.
- (35) Mahato, P.; Mishra, S. K.; Murmu, M.; Murmu, N. C.; Hirani, H.; Banerjee, P. A prolonged exposure of Ti-Si-B-C nanocomposite coating in 3.5wt% NaCl solution: Electrochemical and morphological analysis. *Surf. Coat. Technol.* **2019**, *375*, 477–488.
- (36) Oguzie, E. E.; Oguzie, K. L.; Akalezi, C. O.; Udeze, I. O.; Ogbulie, J. N.; Njoku, V. O. Natural Products for Materials Protection: Corrosion and Microbial Growth Inhibition Using Capsicum frutescens Biomass Extracts. *ACS Sustainable Chem. Eng.* **2013**, *1*, 214–225.
- (37) Corrales-Luna, M.; Le Manh, T.; Romero-Romo, M.; Palomar-Pardavé, M.; Arce-Estrada, E. M. 1-ethyl 3-methylimidazolium thiocyanate ionic liquid as corrosion inhibitor of API SL X52 steel in H₂SO₄ and HCl media. *Corros. Sci.* **2019**, *153*, 85–99.
- (38) Chen, W.; Huang, D. X.; Wei, F. Inhibition Effect of Brainea Insignis Extract Against Carbon Steel Corrosion in HCl Solution. *J. Chin. Soc. Corr. Pro.* **2021**, *41*, 376–382.
- (39) Cao, S.; Liu, D.; Ding, H.; Wang, J.; Lu, H.; Gui, J. Task-specific Ionic Liquids as corrosion inhibitors on carbon steel in 0.5 M HCl solution: An experimental and theoretical study. *Corros. Sci.* **2019**, *153*, 301–313.
- (40) Abdel-Gaber, A. M.; Khamis, E.; Abo-ElDahab, H.; Adeel, S. Inhibition of aluminium corrosion in alkaline solutions using natural compound. *Mater. Chem. Phys.* **2008**, *109*, 297–305.
- (41) Singh, A.; Ansari, K. R.; Banerjee, P.; Murmu, M.; Quraishi, M. A.; Lin, Y. Corrosion inhibition behavior of piperidinium based ionic liquids on Q235 steel in hydrochloric acid solution: Experimental, density functional theory and molecular dynamics study. *Colloids Surf., A* **2021**, *623*, 126708.
- (42) Pathan, S.; Ahmad, S. s-Triazine Ring-Modified Waterborne Alkyd: Synthesis, Characterization, Antibacterial, and Electrochemical Corrosion Studies. *ACS Sustainable Chem. Eng.* **2013**, *1*, 1246–1257.
- (43) Solomon, M. M.; Gerengi, H.; Kaya, T.; Umoren, S. A. Performance Evaluation of a Chitosan/Silver Nanoparticles Composite on St37 Steel Corrosion in a 15% HCl Solution. *ACS Sustainable Chem. Eng.* **2017**, *5*, 809–820.
- (44) Murmu, M.; Saha, S. K.; Bhaumick, P.; Murmu, N. C.; Hirani, H.; Banerjee, P. Corrosion inhibition property of azomethine functionalized triazole derivatives in 1mol L⁻¹ HCl medium for mild steel: Experimental and theoretical exploration. *J. Mol. Liq.* **2020**, *313*, 113508.
- (45) Negm, N. A.; Zaki, M. F.; Said, M. M.; Morsy, S. M. Inhibitory action of biodegradable modified vanillin on the corrosion of carbon steel in 1 M HCl. *Corros. Sci.* **2011**, *53*, 4233–4240.
- (46) Adesina, A. Y.; Gasem, Z. M.; Kumar, A. M. Corrosion resistance behavior of single-layer cathodic arc PVD nitride-base coatings in 1M HCl and 3.5 pct NaCl solutions. *Metall. Mater. Trans. B* **2017**, *48*, 1321–1332.
- (47) Abd El-Lateef, H. M. Corrosion inhibition characteristics of a novel salicylidene isatin hydrazine sodium sulfonate on carbon steel in HCl and a synergistic nickel ions additive: A combined experimental and theoretical perspective. *Appl. Surf. Sci.* **2020**, *501*, 144237.
- (48) Haruna, K.; Saleh, T. A.; Obot, I. B.; Umoren, S. A. Cyclodextrin-based functionalized graphene oxide as an effective corrosion inhibitor for carbon steel in acidic environment. *Prog. Org. Coat.* **2019**, *128*, 157–167.
- (49) Murmu, M.; Saha, S. K.; Murmu, N. C.; Banerjee, P. Effect of stereochemical conformation into the corrosion inhibitive behaviour of double azomethine based Schiff bases on mild steel surface in 1 mol L⁻¹ HCl medium: An experimental, density functional theory and molecular dynamics simulation study. *Corros. Sci.* **2019**, *146*, 134–151.
- (50) Negm, N. A.; Al Sabagh, A. M.; Migahed, M. A.; Bary, H. M. A.; El Din, H. M. Effectiveness of some diquaternary ammonium surfactants as corrosion inhibitors for carbon steel in 0.5 M HCl solution. *Corros. Sci.* **2010**, *52*, 2122–2132.
- (51) Döner, A.; Yüce, A. O.; Kardaş, G. Inhibition effect of Rhodanine-N-Acetic acid on copper corrosion in acidic media. *Ind. Eng. Chem. Res.* **2013**, *52*, 9709–9718.
- (52) Khaled, K. F.; Al-Qahtani, M. M. The inhibitive effect of some tetrazole derivatives towards Al corrosion in acid solution: chemical, electrochemical and theoretical studies. *Mater. Chem. Phys.* **2009**, *113*, 150–158.
- (53) Solmaz, R.; Kardaş, G.; Çulha, M.; Yazıcı, B.; Erbil, M. Investigation of adsorption and inhibitive effect of 2-mercaptothiazoline on corrosion of mild steel in hydrochloric acid media. *Electrochim. Acta* **2008**, *53*, S941–S952.
- (54) Sang, X. J.; Li, J. S.; Zhang, L. C.; Wang, Z. J.; Chen, W. L.; Zhu, Z. M.; Su, Z. M.; Wang, E. B. A novel carboxyethyltin functionalized sandwich-type germanotungstate: synthesis, crystal structure, photo-sensitivity, and application in dye-sensitized solar cells. *Appl. Mater. Interfaces* **2014**, *6*, 7876–7884.
- (55) Sang, X. J.; Li, J. S.; Zhang, L. C.; Zhu, Z. M.; Chen, W. L.; Li, Y. G.; Su, Z. M.; Wang, E. B. Two carboxyethyltin functionalized polyoxometalates for assembly on carbon nanotubes as efficient counter electrode materials in dye-sensitized solar cells. *Chem. Commun.* **2014**, *50*, 14678–14681.
- (56) Sun, H.; Guo, L. Y.; Li, J. S.; Bai, J. P.; Su, F.; Zhang, L. C.; Sang, X. J.; You, W. S.; Zhu, Z. M. Two new armtype polyoxometalates grafted on titanium dioxide films: towards enhanced photoelectrochemical performance. *ChemSusChem* **2016**, *9*, 1125–1133.
- (57) Xu, W.; Han, E.-H.; Wang, Z. Effect of tannic acid on corrosion behavior of carbon steel in NaCl solution. *J. Mater. Sci. Technol.* **2019**, *35*, 64–75.
- (58) Guo, L. Y.; Li, Y.; Zhang, Y.; Li, J.-S.; You, W.-S.; Su, F.; Zhu, Z.-M.; Sang, X.-J.; Zhang, L.-C. Extended visible photosensitivity of carboxyethyltin functionalized polyoxometalates with common organic dyes enabling enhanced photoelectric performance. *RSC Adv.* **2017**, *7*, 20685–20693.
- (59) Miao, M. Y.; Wang, J. H.; Hu, W. B. Synthesis, characterization and inhibition properties of ZnAlCe layered double hydroxide intercalated with 1-hydroxyethylidene-1,1-diphosphonic acid. *Colloids Surf., A* **2018**, *543*, 144–154.
- (60) Yamashita, T.; Hayes, P. Analysis of XPS spectra of Fe²⁺ and Fe³⁺ ions in oxide materials. *Appl. Surf. Sci.* **2008**, *254*, 2441–2449.
- (61) Caglar, Y.; Caglar, M.; Ilican, S. XRD, SEM, XPS studies of Sb doped ZnO films and electrical properties of its based Schottky diodes. *Optik* **2018**, *164*, 424–432.
- (62) Xie, F. Y.; Gong, L.; Liu, X.; Tao, Y. T.; Zhang, W. H.; Chen, S. H.; Meng, H.; Chen, J. XPS studies on surface reduction of tungsten oxide nanowire film by Ar⁺ bombardment. *J. Electron Spectrosc. Relat. Phenom.* **2012**, *185*, 112–118.
- (63) Wan, K.; Feng, P.; Hou, B.; Li, Y. Enhanced corrosion inhibition properties of carboxymethyl hydroxypropyl chitosan for mild steel in 1.0 M HCl solution. *RSC Adv.* **2016**, *6*, 77515–77524.
- (64) Bösing, M.; Loose, I.; Pohlmann, H.; Krebs, B. New strategies for the generation of large heteropolymetalate clusters: the β-B-SbW₉ fragment as a multifunctional unit. *Chem. – Eur. J.* **1997**, *3*, 1232–1237.
- (65) Botar, B.; Yamase, T.; Ishikawa, E. A highly nuclear vanadium-containing tungstobismutate: synthesis and crystal structure of K₁₁H[(BiW₉O₃₃)₃Bi₆(OH)₃(H₂O)₃V₄O₁₀].25H₂O. *Inorg. Chem. Commun.* **2000**, *3*, 579–584.
- (66) Hutton, R. E.; Burley, J. W.; Oakes, V. β-substituted alkyltin halides: I. Monoalkyltin trihalides: synthetic, mechanistic and spectroscopic aspects. *J. Organomet. Chem.* **1978**, *156*, 369–382.